Time-delayed interactions on acoustically driven bubbly screens

Yuzhe Fan, Haisen Li, Daniel Fuster

Time-delayed interactions on acoustically driven bubbly screens

Yuzhe Fan,[1, 2, 3] Haisen Li,[1, 2, 3] and Daniel Fuster[4, a]

[1]*College of Underwater Acoustic Engineering, Harbin Engineering University,*

Harbin 150001,China

[2]*Key Laboratory of Marine Information Acquisition and Security(Harbin*

Engineering University), Ministry of Industry and Information Technology,

Harbin 150001, China

[3]*Acoustic Science and Technology Laboratory, Harbin Engineering University,*

Harbin 150001, China

[4]*Sorbonne Universités, UPMC Univ Paris 06, CNRS, UMR 7190,*

Institut Jean Le Rond d'Alembert, F-75005 Paris, France

(Dated: 13 August 2021)

We discuss the influence of compressibility effects including time delay on the dynamics of acoustically excited bubbly screens. In the linear regime, we show that the proposed model recovers the results from the effective medium theory up to second order for infinite bubbly screens when the wavelength is large compared to the inter-bubble distance, and bubbles are equally spaced without the need of introducing any fitting parameter. The effect of boundaries on finite size screens and randomization on the bubble position is shown to lead to the appearance of multiple local resonances and characteristic periodic structures. In the non-linear regime, we treat time-delay effects as a delay-differential equation that is directly solved numerically. We show the appearance the optimal distance for subharmonic emission for crystal structures and discuss the accuracy of effective medium theories in the strong non-linear regime.

[a]fuster@dalembert.upmc.fr

I. INTRODUCTION

The dynamics of cavities in liquids has attracted a lot of interest over the past few decades (Fuster, 2019; Lohse, 2018). The oscillation of an isolated bubble is well described by the Rayleigh-Plesset (RP) like equations that account for compressibility effects (Gilmore, 1952; Keller and Miksis, 1980; Lauterborn and Kurz, 2010; Prosperetti *et al.*, 1986). However, bubbles often appear in ensembles, and bubble-bubble interactions need to be accounted for as the bubble interface acceleration influences the pressure distribution in the bubble surroundings. One traditional way to account for the influence of interactions is to use the effective medium method. Foldy (1945), Caflisch *et al.* (1985), and Commander and Prosperetti (1989) consider the influence that the dynamic bubble response have on the effective properties of a wave propagating in a bubbly liquid. The multiple interactions among bubbles are described by the interaction between each bubble and the averaged pressure field. However these models are limited to diluted systems and frequencies for which the wavelength is larger than the characteristic bubble radius and the inter-bubble distance.

In an attempt to generalize the range of applicability of these theories to shorter wavelengths and capture more accurately the interaction mechanisms among bubbles, some authors propose to solve a coupled system of RP like equations (Fan *et al.*, 2020b; Fuster and Colonius, 2011; Ilinskii *et al.*, 2007; Mettin *et al.*, 1997). These approaches can be eventually coupled with an Eulerian–Lagrangian approach (Fuster and Colonius, 2011; Maeda and Colonius, 2019) to capture both, short and long wave range interactions and can be

3

considered as two-way coupled model, where bubbles can directly feel the acoustic field emitted by each other. An intrinsic difficulty in these models is how to account for the influence of the liquid compressibility on the multiple interactions among bubbles. Indeed one of the most frequently-used assumption is to resort to the incompressible limit where the interactions among bubbles takes place instantaneously neglecting any time-delay effect due to liquid compressibility. Although this assumption is certainly valid when the wavelength of the excitation pressure wave is much larger than the characteristic size of the bubble cluster, the accuracy and degree of applicability of these models in systems with many bubbles has not been discussed in detail.

Some numerical studies applied to medical related research such as high-intensity focused ultrasound (Okita *et al.*, 2013), ultrasound contrast agent (Faez *et al.*, 2012), and drug delivery (Coussios and Roy, 2008) point out the importance of compressibility effects, an in particular time-delay effects in real applications (Sujarittam and Choi, 2020). More fundamental studies including experimental works studying the acoustic propagation in the vicinity of a bubble chain (Manasseh *et al.*, 2004) have shown that the time-delay effects considerably change the resonance frequencies and the damping factors of the effective medium (Doinikov *et al.*, 2005; Ooi *et al.*, 2008), so does bubble near boundaries (Dahl and Kapodistrias, 2003; van't Wout and Feuillade, 2021; Ye and Feuillade, 1997). In the context of the development of acoustic metamaterials, two-dimensional bubble layers also known as bubbly screens have also became a widely investigated system since 2009 in a series of papers published by Leroy and coworkers (Leroy *et al.*, 2015, 2009; Lombard *et al.*, 2015).

Using the self-consistent approach based on the effective medium theory, the transmission and reflection coefficient measured experimentally in the linear regime can be well captured by accounting for the influence of time-delay effects on the interaction term among bubbles. In non-linear regime, the asymptotic analysis based on effective medium theory (Miksis and Ting, 1989; Pham *et al.*, 2021) have shed light into the role of compressibility on the mechanisms of multiple interactions among bubbles. However, these models still face some challenges. For example it is known that, even in the dilute limit, crystal configuration have special acoustic properties (Devaud *et al.*, 2010). The capability of these models to distinguish between the properties of specific configurations (e.g. crystals) and the ensemble average of randomly distributed systems has not been clarified . Also, it is not clear how well averaged models capture the influence of boundary effects as well as polydispersity effects.

In this work we discuss the applicability and accuracy of models based on the resolution of a coupled system of RP like equations to capture the response of bubbly screens (Figure 1). After presenting a particularization of the system of Rayleigh-Plesset like equations proposed in Fuster and Colonius (2011) to solve for the dynamic response of the bubbles, we show that this model is able to recover the second order solution predicted by the effective medium theory in the linear oscillating regime without the need of introducing any fitting parameter. Then the influence of boundary effects and randomness on the accuracy of the predictions from the effective medium theory are discussed in the linear regime. In the non-linear regime, we present numerical results of the solution of the system of equations using a delay-

77 differential equation solver showing examples that reveal the importance of compressibility

78 effects to correctly predict the bubble dynamic response.

II. BUBBLY SCREEN MODEL

80   The dynamics of an oscillating spherical bubble is described using the Keller-Miksis like

81 equation (Keller and Miksis, 1980) which is a differential equation for the bubble radius of

82 the ith bubble in a weakly compressible liquid characterized by its speed of sound c and

83 density ρ

$$\rho\left(R_i\ddot{R}_i\left(1-\frac{\dot{R}_i}{c}\right)+\frac{3\dot{R}_i^2}{2}\left(1-\frac{\dot{R}_i}{3c}\right)\right)-\left(1+\frac{\dot{R}_i}{c}+\frac{R_i}{c}\frac{d}{dt}\right)(p_{i,B}-p_\infty)=\rho I_i(t_d). \quad (1)$$

84 In the equation above, $p_\infty(t)=p_0+f(t)$ is the pressure excitation, $p_{i,B}$ is the liquid pres-

85 sure at the interface of the ith bubble, which we describe using a simple polytropic law

86 $p_{i,B}=\left(p_0+\frac{2\sigma}{R_{i,0}}\right)\left(\frac{R_{i,0}}{R_i}\right)^{3\kappa}-\frac{2\sigma}{R_i}-\frac{4\mu\dot{R}_i}{R_i}$, where p_0 is the static pressure; $R_{i,0}$ is the ith bubble

87 radius at equilibrium; σ is the surface tension; μ is the liquid viscosity.

88

89   The interaction term $I(t_d)$ represents the pressure fluctuation induced by the presence

90 of the surrounding bubbles, which has to be evaluated at the deferred time $t_d=t-d_{ij}/c$,

91 where $d_{ij}=|\vec{x}_i-\vec{x}_j|$ represents the distance from the ith bubble located at $\vec{x}_i$ to the jth

92 bubble located at $\vec{x}_j$. Following Fuster and Colonius (2011), it can be readily shown that

$$I_i=I_{i,0}+I_{i,1}, \quad (2)$$

where both terms have to be evaluated at the deferred time t_d

$$I_{i,0}(t_d) = -\sum_{j \neq i}^{N} \frac{R_j}{D_{ij}} \left(R_j \ddot{R}_j + 2\dot{R}_j^2 \right),$$

$$I_{i,1}(t_d) = -\frac{1}{c} \left[\sum_{j \neq i}^{N} \frac{R_j}{D_{ij}} \dot{R}_j \left[R_j \ddot{R}_j + \frac{\dot{R}_j^2}{2} - \frac{(p_{j,B} - p_\infty)}{\rho} \right] - \sum_{j \neq i}^{N} \frac{R_j^2}{D_{ij}} \frac{d}{dt} \frac{(p_{j,B} - p_\infty)}{\rho} + \dot{R}_i I_{i,0} \right] (3)$$

In the equations above, we only keep first order compressibility correction terms in the

intensity of the collapse of bubbles, which scale as a function of the Mach number $Ma = \frac{\dot{R}}{c}$,

and time-delay effects. Neglecting time-delay effects (e.g. $t_d = t$) leads to a coupled system

of equations that needs to be solved. In the limit of $c \to \infty$ we recover the classical form of

the interaction term $I_i \approx I_{i,0}$ evaluated at t (Bremond *et al.*, 2006; Ida *et al.*, 2007; Yasui

et al., 2008). Otherwise, as explained in Section IV, it is required to solve a differential

equation with time delay.

III.   COMPRESSIBILITY EFFECTS IN THE LINEAR OSCILLATION REGIME

A.   General case

In this section, we start considering the dynamics of a finite bubbly screen with monodis-

perse bubbles excited by a weak perturbation, where $R_{i,0} = R_{j,0} = R_0$. Bubbles are arranged

in N_l layers in the $x = 0$ plane ($N_l = 3$ in Figure 1). For a system with N bubbles of the

same equilibrium radius, the coupled set of equations that needs to be solved is

$$R_i \ddot{R}_i - \left(1 + \frac{R_i}{c} \frac{d}{dt} \right) \frac{p_{i,B} - p_\infty}{\rho} = -\sum_{j \neq i}^{N} \frac{R_j^2(t_d)}{d_{ij}} \ddot{R}_j(t_d) + \sum_{j \neq i}^{N} \frac{R_j(t_d)}{d_{ij}} \frac{R_j(t_d)}{c} \frac{d}{dt} \frac{(p_{j,B}(t_d) - p_\infty(t_d))}{\rho},$$
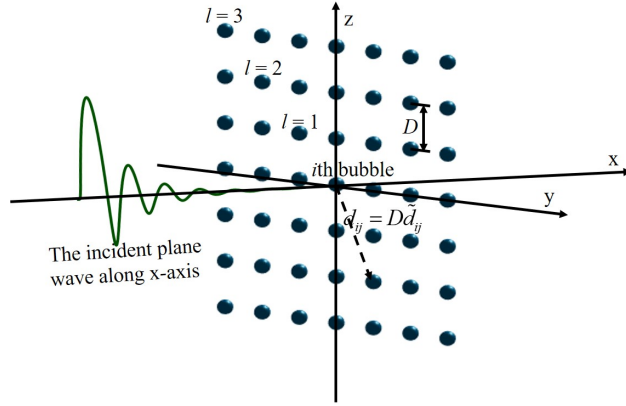
$$(4)$$

FIG. 1. A typical crystal distributed bubbly screen located at $x = 0$ plane.

where $R_i(t) = R_0(1 + r'_i e^{\iota\omega t})$, $R_i(t_d) = R_0(1 + r'_i e^{\iota\omega(t - d_{ij}/c)})$. For simplicity, we consider a planar wave such that $p_\infty = p_0(1 + p' e^{\iota\omega t})$, neglect viscous, thermal, and surface tension terms during linear analysis, and thus have $p_{i,B} - p_0 = -3\gamma p_0 r'_i e^{\iota\omega t}$. For a given physical system at constant reference pressure, the dimensionless wavenumber $kR_0 = \frac{\omega}{\omega_0}\frac{1}{c}\sqrt{\frac{3\kappa p_0}{\rho}}$ depends on the frequency ratio between the excitation frequency, ω, and the resonance frequency of single isolated oscillating bubble $\omega_0 = \sqrt{\frac{3\gamma p_0}{R_0^2 \rho}}$. For air bubbles in water at atmospheric conditions $\frac{1}{c}\sqrt{\frac{3\kappa p_0}{\rho}} \approx 10^{-2}$ and therefore $kR_0 < 1$ is usually a reasonable assumption. This parameter will be held constant in what follows, where we show the solution for particular configurations of the bubbly screen. We can also define an alternative dimensionless wavenumber using the averaged inter-bubble distance D as $kD = \frac{D}{R_0}\frac{\omega}{\omega_0}\frac{1}{c}\sqrt{\frac{3\kappa p_0}{\rho}}$, which is not always small in diluted systems.

A first remark is that, in the linear regime, the influence of the compressibility correction term in the interaction is not null, and it is not sufficient to retain the incompressible

8

interaction term only. Neglecting terms of order $(kR_0)^2$, the set of equations above can be written in matrix form as

$$(\mathbf{A}^{(0)} + \imath k R_0 \mathbf{A}^{(1)})\vec{r'} = \vec{B}p',$$

119 where the coefficients of the matrices $\mathbf{A}^{(0)}$ and $\mathbf{A}^{(1)}$ and vector $\vec{B}$ are defined introducing

120 the local variable $\mathfrak{K}_i = \frac{R_0}{D}\sum_{j\neq i}^N \frac{e^{-\imath k D \tilde{d}_{ij}}}{\tilde{d}_{ij}}$, the wavenumber $k = \omega/c$ and the nondimensional

121 distance $\tilde{d}_{ij} = |\vec{x}_i - \vec{x}_j|/D$ (see appendix A for the full expressions).

122

If we only consider the solution of a planar incident wave, this linear set of equations can

be numerically solved for an arbitrary constant value of the RHS to find all r'_i. Once these

values are obtained, we can define the complex quantity

$$Q_i^* = \frac{\sum_{j\neq i}^N (r'_i - r'_j)\frac{e^{-\imath k D \tilde{d}_{ij}}}{\tilde{d}_{ij}}}{r'_i \sum_{j\neq i}^N \frac{e^{-\imath k D \tilde{d}_{ij}}}{\tilde{d}_{ij}}}$$

123 to express the solution of the system as

$$F_i(\omega/\omega_0)r'_i = -\frac{p_0}{\rho R_0^2 \omega_0^2}p', \tag{5}$$

124 where

$$F_i(\omega/\omega_0) = 1 - \left(\frac{\omega}{\omega_0}\right)^2 - \left(\frac{\omega}{\omega_0}\right)^2 K_i^* \tag{6}$$

125 is defined for each bubble depending on the complex function

$$K_i^* = \mathfrak{K}_i(1 - Q_i^*) - \imath k R_0 \left[(1 + \mathfrak{K}_i)^2 - \mathfrak{K}_i Q_i^*\left(1 + \mathfrak{K}_i + \frac{\omega_0^2}{\omega^2}\right)\right]. \tag{7}$$

126 The real and imaginary parts of K_i^* are typically used to define the resonance frequency

127 $\omega_{i,res}$ and the damping coefficient ζ_i for the ith bubble as

$$\omega_{i,res}^2 = \frac{\omega_0^2}{1 + \Re(K_i^*)}; \qquad \zeta_i = -\Im(K_i^*). \tag{8}$$

9

It is easy to verify that, when $\mathfrak{K}_i \to 0$, we recover the limit of an isolated bubble where $\omega_{i,res} = \omega_0$ and $\zeta_i = \zeta_0 = kR_0$ representing the acoustical damping of a single bubble due to compressibility effects.

For systems where F_i is not uniform for all the bubbles, multiple local resonances (corresponding to zeros of the real part of F_i function) appear. Writing an equation for the bubble volume evolution, $V_i = V_0(1 + V_i' e^{\iota \omega t})$ with V_0 the bubble volume at equilibrium, we can define a global resonance and a global damping factor using the averaged change of gas volume per bubble

$$\frac{V_0}{N} \sum_{i=1}^{N} V_i' = \frac{4\pi R_0^3}{N} \sum_{i=1}^{N} r_i' = -\frac{4\pi R_0 p_0}{\rho_l \omega_0^2} < \frac{1}{F_i} > p'$$

which can be also written as

$$\frac{1}{< \frac{1}{F_i} >} \frac{1}{N} \sum_{i=1}^{N} r_i' = -\frac{p_0}{\rho_l R_0^2 \omega_0^2} p', \tag{9}$$

where $< \frac{1}{F_i} >= \frac{1}{N} \sum_{i=1}^{N} \frac{1}{F_i(\omega/\omega_0)}$ denotes the average over all the bubbles in the screen. By introducing an averaged coefficient K^* defined from

$$\frac{1}{< \frac{1}{F_i} >} = 1 - \left(\frac{\omega}{\omega_0}\right)^2 - \left(\frac{\omega}{\omega_0}\right)^2 K^*,$$

the global resonance and the global damping factor based on the definitions in Eq. 8 are given as:

$$\omega_{res}^2 = \frac{\omega_0^2}{1 + \Re(K^*)}; \qquad \zeta = -\Im(K^*). \tag{10}$$
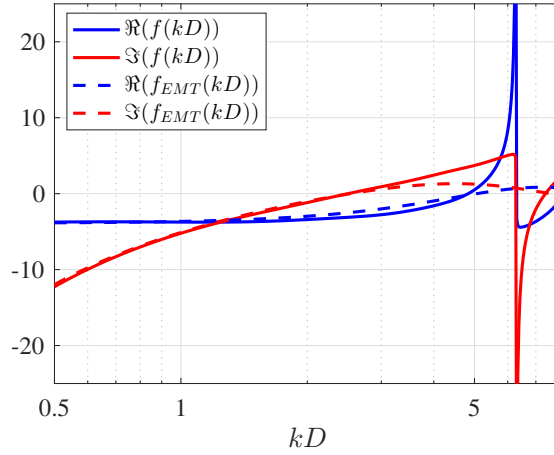
10

FIG. 2. Real and imaginary part of the function $f(kD)$. For reference we include the predictions of the effective medium theory. The solid line is corresponding to the $f(kD)$ and the dashed line is corresponding to EMT. The blue line is the real part, and the red line is the imaginary part. $N_l = 12000$ is used to keep $f(kD)$ converge.

B. Synchronous solution for an infinite bubbly screen with crystal configuration

We start considering the synchronous solution with equal amplitude for all bubbles ($Q_i^* = 0$ for all bubbles). In this limit the solution of the system is given by the simplified expression of $F_i \to F$

$$F(\omega/\omega_0) = 1 - \left(\frac{\omega}{\omega_0}\right)^2 - \left(\frac{\omega}{\omega_0}\right)^2 (\mathfrak{K} - \imath k R_0 (1 + \mathfrak{K})^2), \tag{11}$$

where $\mathfrak{K}_i \to \mathfrak{K} = \frac{R_0}{D} f(kD)$ is a function that is proportional to the bubble inter-spacing parameter R_0/D and the function

$$f(kD) = \sum_{j \neq i}^{\infty} \frac{e^{-\imath k D \tilde{d}_{ij}}}{\tilde{d}_{ij}}, \tag{12}$$

11

which depends on the dimensionless wavenumber kD and the particular geometry considered only. In the particular case of the crystal structure represented in Figure 1, $f(kD)$ becomes

$$f(kD) = \sum_{l=1}^{\infty} \frac{4}{l} e^{-\imath k D l} \left(1 + \sum_{q=1}^{l} \frac{2}{\sqrt{1+(q/l)^2}} e^{\imath k D l (1-\sqrt{1+(q/l)^2})} \right), \tag{13}$$

which needs to be evaluated numerically except in very particular cases. For instance for $kD = 2\pi n$, with n being an integer, the first term is a diverging harmonic series implying zero resonance frequency and infinite attenuation. We identify this phenomenon with a resonance phenomenon in the cavities within the bubbles. The convergence properties of this series in a general case are discussed in Appendix B. It is interesting to note that the results obtained are in agreement with the expression proposed by Leroy *et al.* (2009) in the small kD limitation neglecting the correction of order $(kR_0 \cdot \mathfrak{K})$ without the need of introducing any fitting parameter. Using an homogeneization approach and introducing a cuttoff length $b = D/\sqrt{\pi}$, Leroy *et al.* (2009) obtain $\mathfrak{K}$ using the bubble density $n_d = 1/D^2$ (number of bubbles per unit area in the screen) as

$$\mathfrak{K}_{\text{EMT}} = \frac{R_0}{D} f_{\text{EMT}}(kD) \approx \int_b^{\infty} \frac{R_0}{r} e^{-\imath k r} 2\pi r n_d dr = -\frac{R_0}{D} f_{\text{EMT}}(kD), \tag{14}$$

$$f_{\text{EMT}}(kD) = \frac{2\pi}{kD} \left(\sin(kb) + \imath \cos(kb) \right). \tag{15}$$

As shown by Pham *et al.* (2021), this expression is similar to the extension of the asymptotic analyses proposed by Caflisch *et al.* (1985) and later extended by Miksis and Ting (1989) to the second order, where the correction due to the collective effects of the bubbly screen is (Pham *et al.*, 2021)

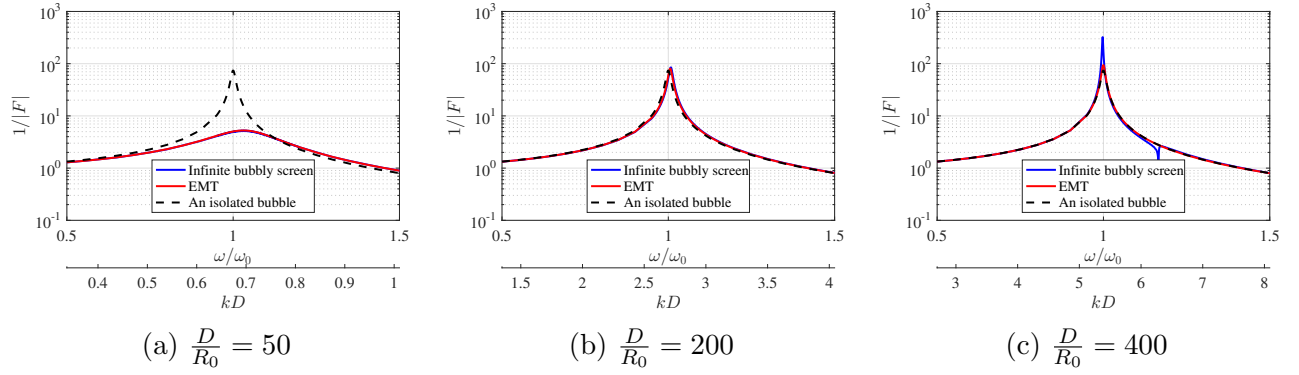$$f_{\text{EMT}}(kD) = -3.9 - \imath \frac{2\pi}{kD}. \tag{16}$$

FIG. 3. $1/|F|$ v.s. ω/ω_0 for three different concentrations. The series are evaluated using $N_l = 12000$ layers.

Using the small angle approximation, it is straightforward to see that eqs. 16 and 15 are equivalent and, as shown in Figure 2, reproduce well the values of the series for $kD \lesssim 3$. In what follows we denote the predictions of this model as effective medium theory (EMT).

Figure 3 represents $1/|F|$ as a function of the frequency for three different concentrations. For high concentrations ($D/R_0 = 50$) the resonance peak is damped, this effect being well captured by the EMT. As the bubble concentration is decreased, the curve tends to recover the result of an isolated bubble. Remarkably, the intensity of the peak at resonance becomes much more important than the one predicted by the EMT for $kD \approx 2\pi$. To gain further insight, Figure 4 shows the influence of D/R_0 at constant forcing frequency on the global resonance and the global damping factor. By changing the inter-bubble distance, the proposed model recovers well the predictions of the effective medium approximation for $kD \lesssim 3$, while for large values of kD both models give different predictions. This discrepancy is attributed to the difference between crystal structure and the random bubble distribution as discussed
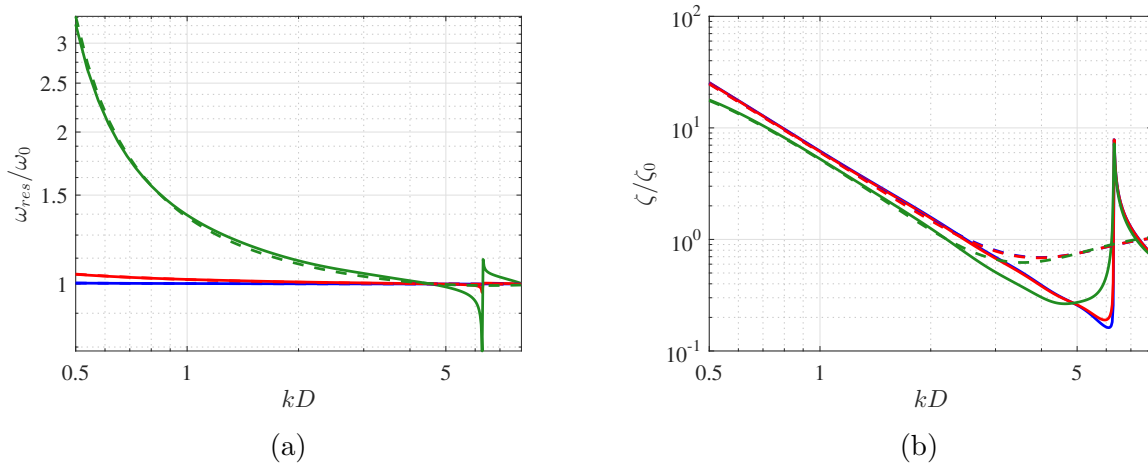
13

FIG. 4. (Left) Concentration effects on ω_{res}/ω_0 and (right) on ζ/ζ_0. Solid lines are used for the approximated exact solution ($N_l = 12000$). Dashed lines represent the solution provided by the effective medium theory. The frequencies used are $\omega/\omega_0 = 0.0785, 0.785, 7.85$ for blue, red and green line respectively.

171 later on for a finite bubbly screen. In the effective medium approximation, bubbles are

172 continuously and homogeneously distributed in the space, and the oscillating term $e^{-ikD\tilde{d}_{ij}}$

173 is thus smoothed out. The current model is able to capture the resonance effects originated

174 for particular configurations. In the particular example shown here, it is expected to find a

175 first resonance for $kD = 2\pi$, corresponding to the appearance of the resonance within the

176 distance between bubbles.

177

178 **C. Finite size bubbly screens**

179   In many applications, the size of the bubbly screens is limited to few tens or hundreds

180 of bubbles, and the infinite screen limit may not be applicable. In addition, these systems
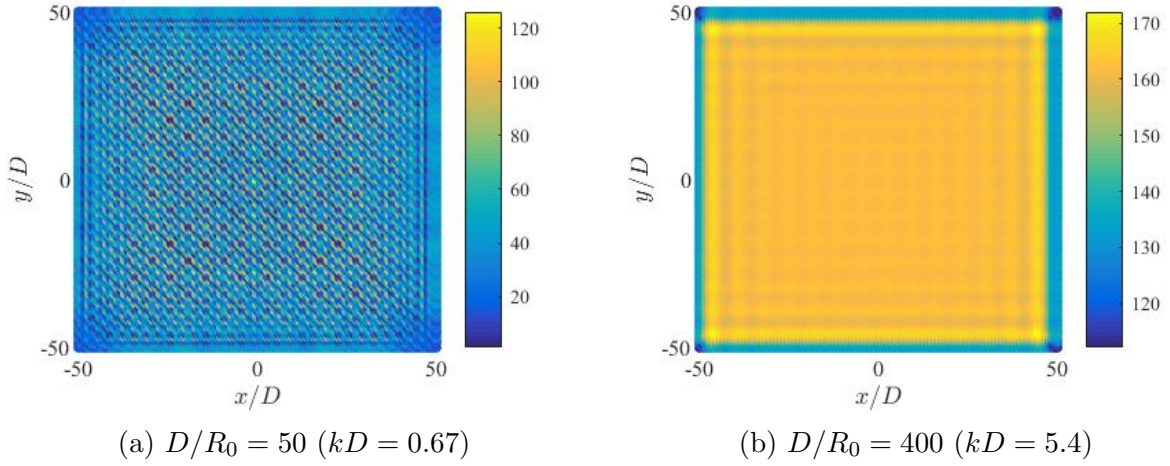
14

(a) $D/R_0 = 50$ ($kD = 0.67$)   (b) $D/R_0 = 400$ ($kD = 5.4$)

FIG. 5. Distribution of $1/|F_i|$ for $\omega/\omega_0 = 1$ in a 101×101 bubbly screen.

present the appearance of multiple resonance frequencies as a consequence of the boundary effects on the dynamics of the bubbles. Figure 5 shows an example of the distribution of function $1/|F_i|$ for a 101×101 bubbly screen excited at the single bubble resonance frequency for two different values of the dimensionless wavenumber: $kD < 1$ and near $kD \approx 2\pi$. This function, which is directly proportional to the intensity of the bubble oscillation, presents characteristic spatial patterns that are especially visible in the diluted limit when $kD \approx 2\pi$ ($D/R_0 = 400$ in this case).

The influence of spatial structures is discussed using variable Q_i^*, which integrates the influence of interactions on the dynamics of a given bubble due to phase lag and amplitude changes among the other bubbles, and tends to zero in the limit of an infinite bubbly screen for crystal configurations. Figure 6 shows that the intensity of the mean value of $|Q_i^*|$ becomes maximum at resonance, tends to a plateau at larger frequencies and quickly decays for low frequencies. Characteristic patterns are easily identified at resonance conditions but also become visible for other values of the forcing frequency. Notice that it also is possible
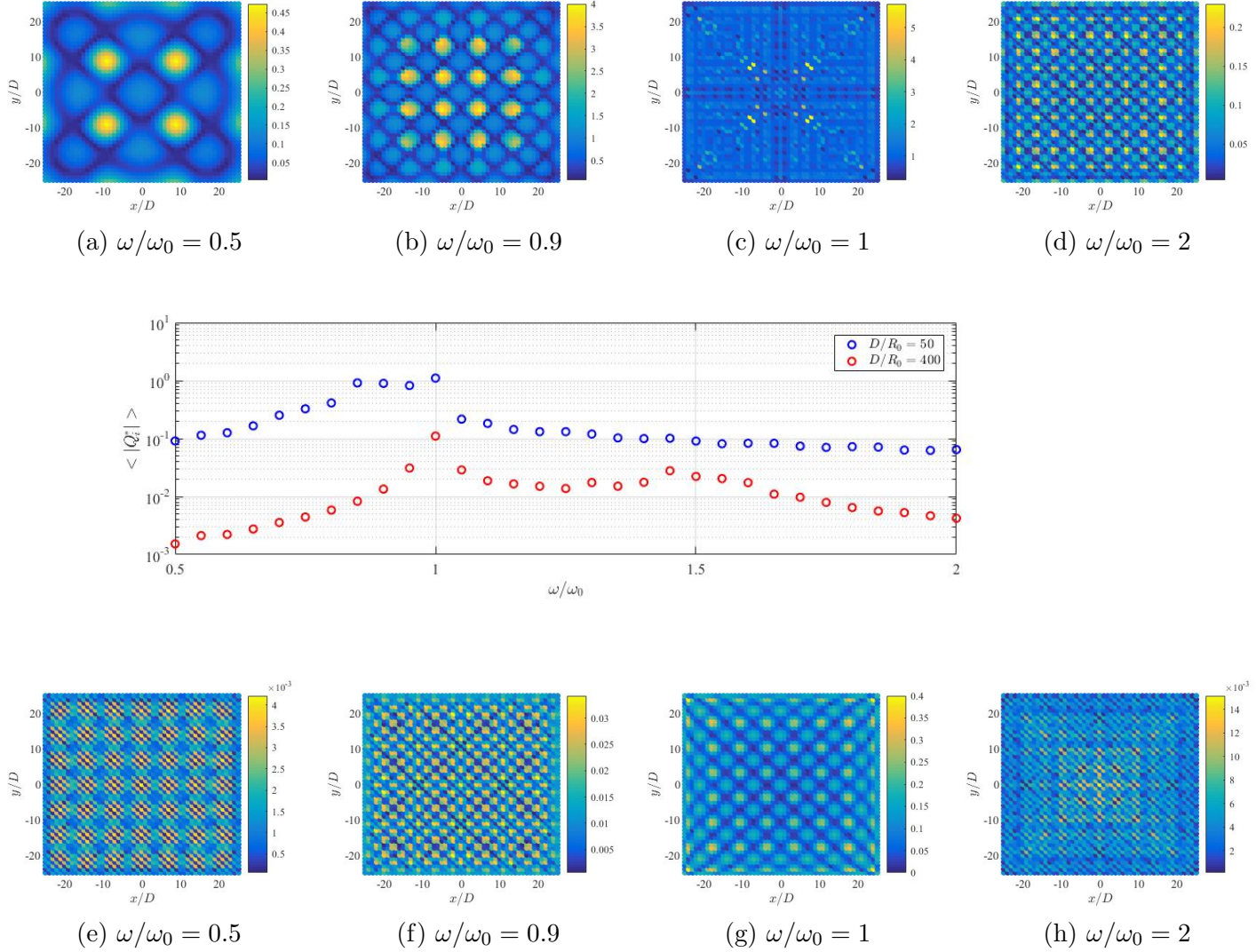
15

(a) $\omega/\omega_0 = 0.5$ (b) $\omega/\omega_0 = 0.9$ (c) $\omega/\omega_0 = 1$ (d) $\omega/\omega_0 = 2$

(e) $\omega/\omega_0 = 0.5$ (f) $\omega/\omega_0 = 0.9$ (g) $\omega/\omega_0 = 1$ (h) $\omega/\omega_0 = 2$

FIG. 6.   The middle Figure shows the mean value of $|Q_i^*|$ of a 51×51 bubbly screen as a function of

frequency for $D/R_0 = 50$ and $D/R_0 = 400$. Top Figures show the $|Q_i^*|$ maps for $D/R_0 = 50$;bottom

ones are corresponding to $D/R_0 = 400$.

to find frequencies at which spatial patterns are difficult to identify (Figure 6c). Besides,

bubble concentration shifts the resonance peak which also leads to a shift in the structures
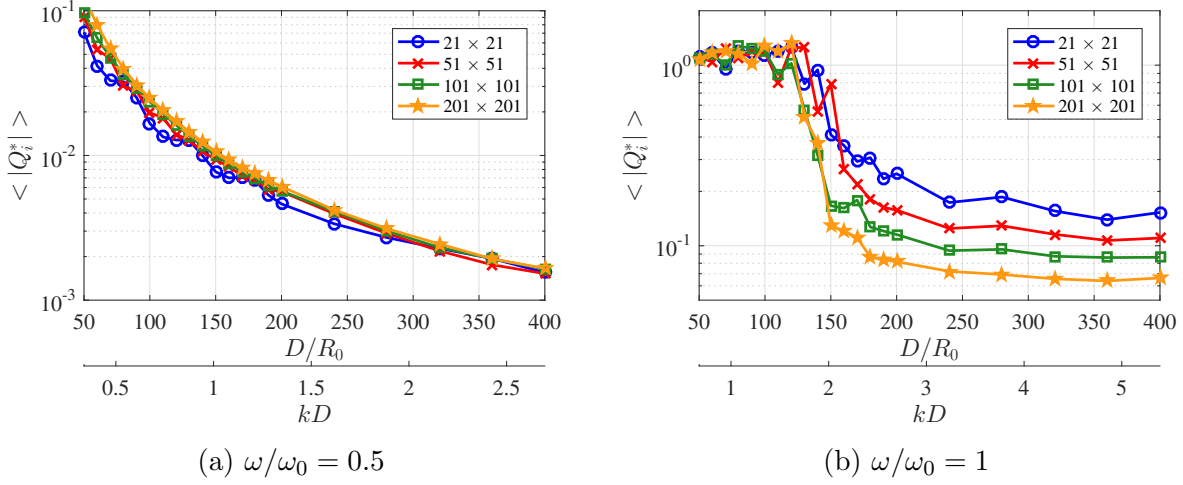
shown for a given frequency (Figure 6).

16

FIG. 7. Influence of concentration on $< |Q_i^*| >$ for various finite size bubbly screens and two different values of ω/ω_0.
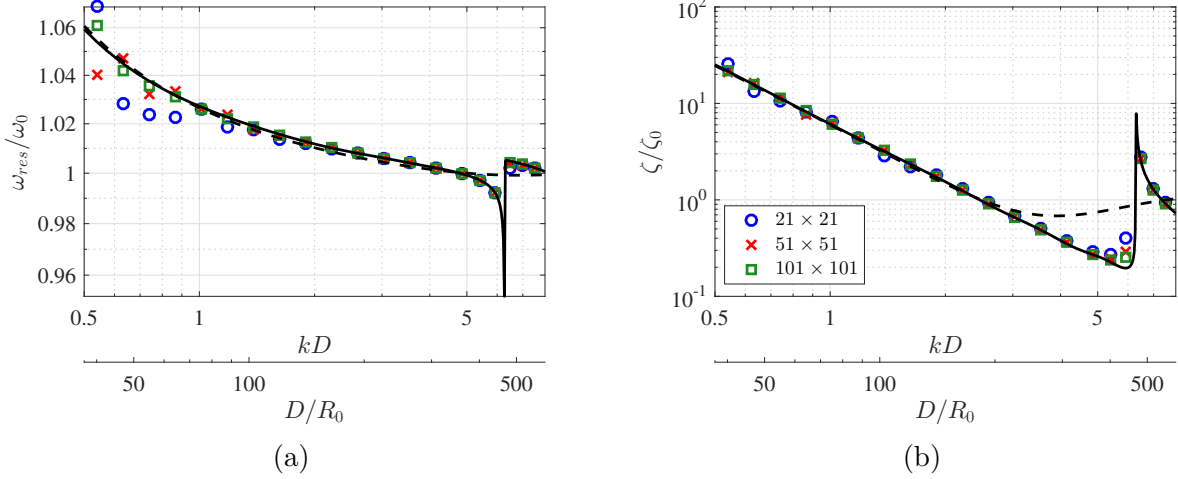

FIG. 8. Global resonance frequency and the global acoustical damping factor of finite bubbly screen with different screen sizes for $\omega/\omega_0 = 1$. 21×21 (blue circle), 51×51 (red cross sign) and 101×101 (green square). The theoretical curves calculated for an infinite system (black solid line, $N_l = 12000$) and effective medium theory are included for reference (dashed line).

17

The role of the concentration on $< |Q_i^*| >$ is shown in Figure 7. At resonance (figure 7b), we observe a sharp transition between $kD \leq 2$, where the fluctuations of $< |Q_i^*| >$ become of order unity, and $kD > 2$, where $< |Q_i^*| >$ takes significantly smaller values. Remarkably, in the regime of $kD \leq 2$, we do not see any clear asymptotic convergence to $< |Q_i^*| > \to 0$ as we increase the number of bubbles in the screen. Below resonance (figure 7a), the value of $< |Q_i^*| >$ is small but no clear convergence to zero is observed for the screens considered. One of the reasons for the slow convergence may be the excitation of non-uniform modes induced by boundary effects. The consequences of perturbation on the plane containing the bubbles in the infinite case (we have imposed an unperturbed planar wave in the y-z plane) is left for future works.

The effect of finite size effects on the global resonance frequency and damping factor can be seen in Figure 8 for $\omega/\omega_0 = 1$. The infinite bubbly screen limit captures accurately the averaged bubble response of the screen, only observing some small disagreement for very concentrated systems, where we have seen the non-uniformity on the bubble response is important.

D. Randomization

We discuss now the influence of the randomness on the position of the bubbles. To that end, we perturb the position of each bubble by a random number $-\Theta < \theta < \Theta$ with respect to the crystal configuration so that ith bubble is located at $\vec{x}_i = (0, y_i^{(c)} + \theta_{y,i} D, z_i^{(c)} + \theta_{z,i} D)$, where the superscript (c) stands for variables corresponding to the crystal configuration.
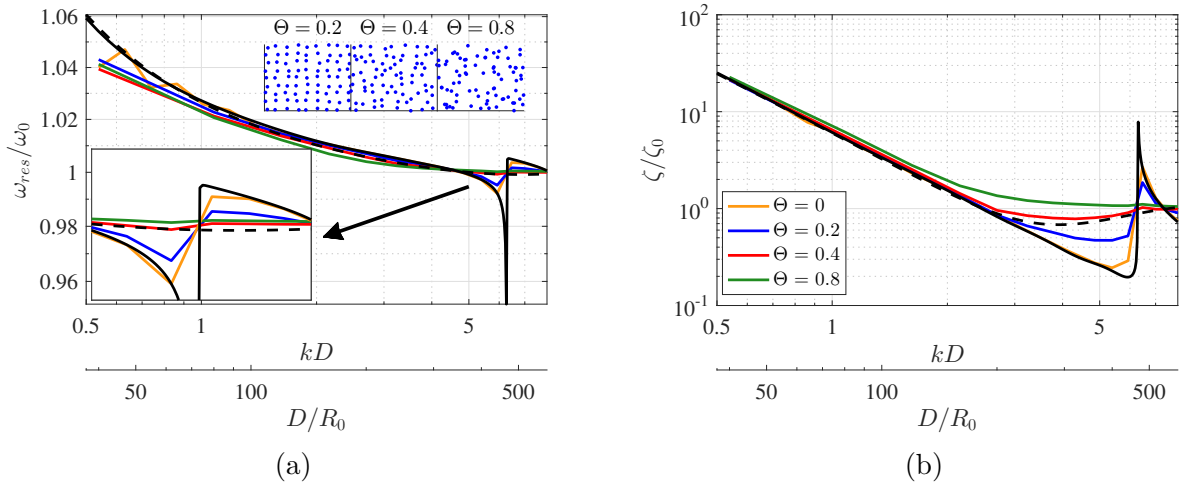
18

FIG. 9. Influence of randomness for (a) the global resonance and (b) the damping coefficient of a finite screen size 51×51 and $\omega/\omega_0 = 1$. An example of the spatial distribution of the bubble positions is given in the inset of (a). For reference we include curves calculated for an infinite system (black solid line, $N_l = 12000$) and effective medium theory (dashed line).

Figure 9 shows the global factors defined in equation 10 averaged over 100 realizations for $\omega/\omega_0 = 1$ using a finite screen with 51×51 bubbles with different concentrations. As expected, the resonance effects observed at $kD = 2\pi$ quickly vanish as the randomization parameter increases. Remarkably, the results obtained differ from the effective medium theory for large values of the randomization parameter and intermediate values of kD, the effect of randomization being especially visible on the effective damping coefficient.

In this case, both matrix $\mathbf{A}^{(0)}$ and matrix $\mathbf{A}^{(1)}$ can be further decomposed as a globally uniform value given by the crystal structure and a correction directly attributed to randomization (see Appendix A). While the expectation of $\mathbf{A}'^{(0)}$ is zero, the non-linear term in the $\mathbf{A}'^{(1)}$ matrix with respect to the position perturbation amplitude makes the averaged response of the system to be different from the crystal situation for small perturbations.

19

For large perturbations, the expectation of both $\mathbf{A}'^{(0)}$ and $\mathbf{A}'^{(1)}$ are a-priori different from zero, and converge to different number with different Θ. In such a situation, the difference between the fluctuation around the crystal configuration and the completely random distribution also makes the averaged response of the system to be different from EMT. In Figure 9 we see that the randomization intensity parameter Θ mainly increases the effective damping for $kD > 1$.

IV. COMPRESSIBILITY EFFECTS IN THE NON-LINEAR REGIME

A. Numerical methods for differential equations with time delay

In the non-linear regime, it is no longer possible to find analytical solutions and one needs to solve the set of ODEs numerically. The differential equations considered can be written as

$$\dot{y}(t) = f(t, y(t), y(t - \tau_1), ..., y(t - \tau_n), \dot{y}(t - \tau_1), ..., \dot{y}(t - \tau_n)), \tag{17}$$

where y is called state variable representing bubble radius or bubble wall velocity in our case. Traditionally, Eq. 17 is usually solved as ordinary differential equations, and the time-delay effect thus has to be ignored ($\tau_1, ..., \tau_n = 0$). In this work, when non-linear effects become important, Eq. 17 is directly solved, treated as neutral delay-differential equation (NDDE), which will reduce to general delay-differential equation (DDE) if $\dot{y}(t) = f(t, y(t), y(t - \tau_1), ..., y(t - \tau_n))$ and extend to state dependent NDDE if any of $(\tau_1, ..., \tau_n)$ is a function of state variable (Bellen and Zennaro, 2013). Integration of DDEs cannot be based on the mere adaption of some standard ODE code to the presence of delayed terms,

20

which may dramatically modify the accuracy and stability of the underlying ODE method.

To deal with NDDE, we first rewrite the Eq. 17 as:

$$\dot{y}(t) = f\left(y(t), y(t-\tau_1), ..., y(t-\tau_n), \frac{y(t-\tau_1) - y(t-\tau_1-\delta_t)}{\delta_t}, ..., \frac{y(t-\tau_n) - y(t-\tau_n-\delta_t)}{\delta_t}\right) \tag{18}$$

which is the dissipative approximation of the NDDE and named as retarded DDE. For small

enough δ_t, the retarded DDE solver will be stable as long as the neutral DDE is stable.

Based on Eq. 18, implicit Runge–Kutta formulas taking advantage of continuous extensions

is used, and the retarded DDE is solved accordingly with residual control. The works of

Shampine (2005, 2008) are recommended for detailed mathematical principles.

B. Numerical results

1. Weakly non-linear regime

One important aspect on the dynamic response of bubbly liquids is the appearance of

subharmonics, which ultimately indicate the first transition route to the chaotic response

obtained for large enough amplitude of excitation (Lauterborn and Cramer, 1981; Lauter-

born and Koch, 1987). The harmonic components of the acoustic wave scattered by bubbles

or ultrasound contrast agents is also important in medical applications (Halldorsdottir *et al.*,

2011; Nio *et al.*, 2019). The harmonics emitted by bubbles has been described by many

authors (see Lauterborn and Kurz (2010) for a review), including studies for contrast agents

in a free field (Andersen and Jensen, 2009; Katiyar and Sarkar, 2011). More recently Fan

et al. (2020a) has revealed the impact of compressibility and bubble-wall interaction effects

on the subharmonic emission of a bubble in a rigid tube. However, the influence of collective

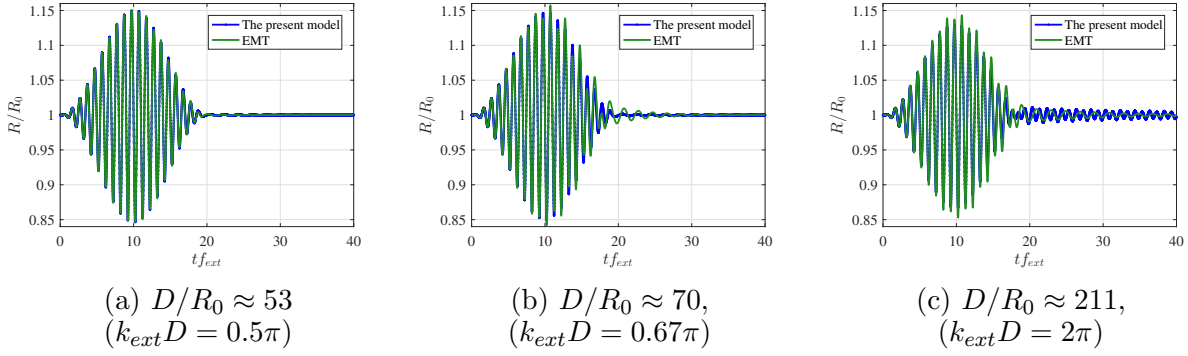(a) $D/R_0 \approx 53$ $(k_{ext}D = 0.5\pi)$

(b) $D/R_0 \approx 70$, $(k_{ext}D = 0.67\pi)$

(c) $D/R_0 \approx 211$, $(k_{ext}D = 2\pi)$

FIG. 10. The radius v.s. time curves. $p_a/p_0 = 2$.

(a) $D/R_0 \approx 53$, $(k_{ext}D = 0.5\pi)$

(b) $D/R_0 \approx 70$, $(k_{ext}D = 0.67\pi)$

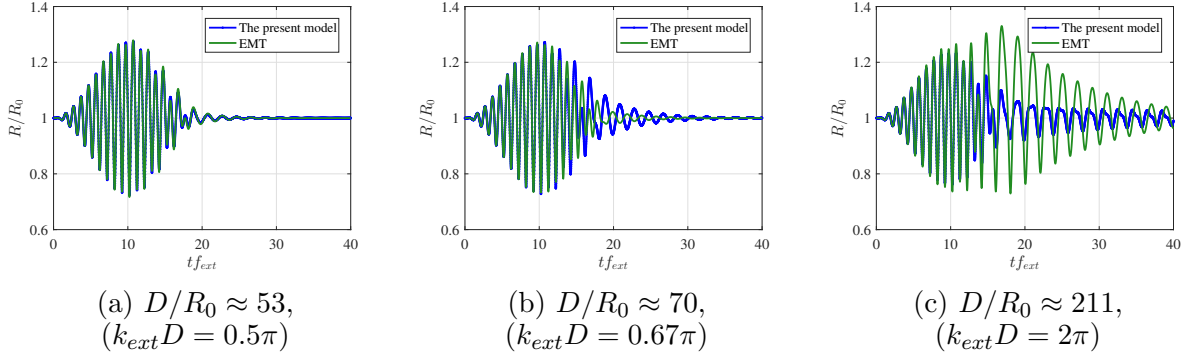(c) $D/R_0 \approx 211$, $(k_{ext}D = 2\pi)$

FIG. 11. The radius v.s. time curves. $p_a/p_0 = 3.5$.

268 effects on the subharmonic emission has not been investigated in detail yet.

269

270   In this section, we compare the results obtained from the model presented for infinite

271 bubbly screens imposing synchronous motion ($R_i = R_j = R$) with the results obtained from

272 the EMT in non-linear regimes (Pham *et al.*, 2021) where

$$I_{EMT} = -2\pi c \dot{R}\frac{R^2}{D^2} + 3.9\frac{R}{D}(2\dot{R}^2 + \ddot{R}R). \qquad (19)$$

273 To that end, we excite the bubbly screen with an incident pulse of the form

$$p_\infty(t) = p_0 - p_a\frac{1}{2}\left[1 - \cos\left(\frac{\omega_{ext}}{N_c}t\right)\right]\sin(\omega_{ext}t), \qquad (20)$$

22

₂₇₄ where $N_c = 20$, and $\omega_{ext} = 2\omega_0$ in order to favor the appearance of a stable subharmonic

₂₇₅ response. For simplicity, in this subsection we will only consider the response of an infinite

₂₇₆ bubble screen.

₂₇₇

₂₇₈ In Figures 10-11, we can see the influence of concentration on the dynamic response of

₂₇₉ an infinite bubbly screen for two different excitation amplitudes. Consistent with the results

₂₈₀ in the linear regime, the effective medium model converges to the present model when the

₂₈₁ value of D/R_0, and therefore, $k_{ext}D$ is small. The differences between two models become

₂₈₂ significant as p_a/p_0 and $k_{ext}D$ increases. Even in the case, where the differences between the

₂₈₃ two models are important (figure 11c), both models fit relatively well for small times, and

₂₈₄ gradually become different only after some time. One explanation could be that in-phase

₂₈₅ and out-phase interactions coming from different layers at different time cancel each other

₂₈₆ and increase oscillatingly. Besides, the fact that the differences between models become

₂₈₇ visible after some time seem to indicate the differences of the EMT and the current model

₂₈₈ on the bifurcation diagrams (Lauterborn and Kurz, 2010).

₂₈₉

₂₉₀ Figure 12 shows the energy in the frequency spectrum of the infinite bubbly screen as a

₂₉₁ function of the bubble concentration from the radiated pressure (Pham et $al.$, 2021):

$$p_{rad} = 2\pi\rho c \frac{R^2\dot{R}}{D^2}. \tag{21}$$

₂₉₂ The energy is calculated as $E = 20log_{10}(\frac{|\mathfrak{F}(p_{rad})|}{|\mathfrak{F}(p_{rad})_{max}|})$, where $\mathfrak{F}(\cdot)$ is the Fourier transform,

₂₉₃ and $|\mathfrak{F}(p_{rad})_{max}|$ is highest energy observed among all simulations. Because the frequency

₂₉₄ of the subharmonic slightly shifts from $\frac{\omega_{ext}}{2}$ with the increasing of the amplitude of the
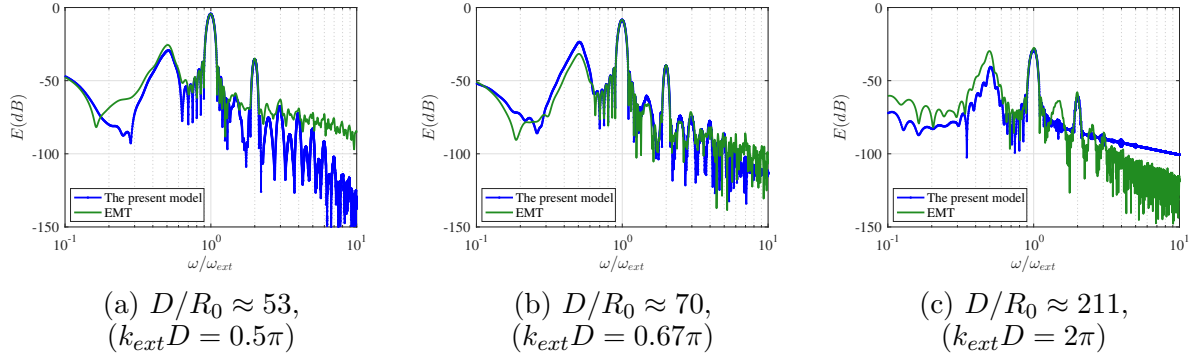
23

(a) $D/R_0 \approx 53$,
$(k_{ext}D = 0.5\pi)$

(b) $D/R_0 \approx 70$,
$(k_{ext}D = 0.67\pi)$

(c) $D/R_0 \approx 211$,
$(k_{ext}D = 2\pi)$

FIG. 12. The frequency spectrum of the present model and EMT using $p_a/p_0 = 3.5$. The energy is calculated by $E = 20log_{10}(\frac{|\mathfrak{F}(p_{rad})|}{|\mathfrak{F}(p_{rad})_{max}|})$, where $|\mathfrak{F}(p_{rad})_{max}|$ is highest energy observed among all simulations.
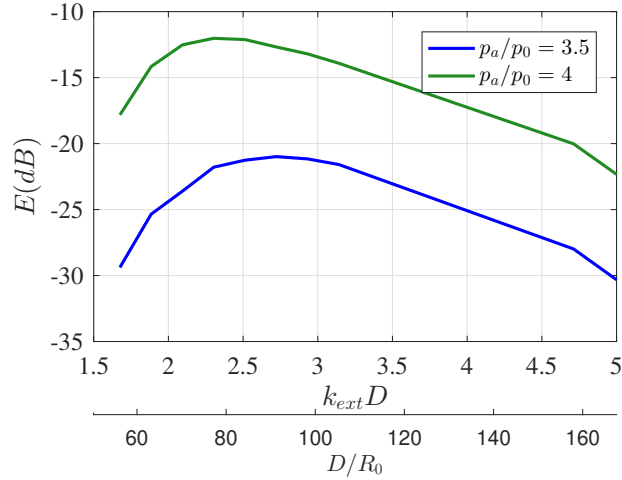

FIG. 13. Energy of the subharmonic as a function of concentration for a constant excitation frequency in a crystal structure.

driving pressure wave, the corresponding energy are chosen according to the peak amplitude rather than energy at $\frac{\omega_{ext}}{2}$. As expected the energy on the fundamental component increases as D/R_0 decreases due to the increase of bubble concentration (Figure 12). The overall spectrum is well reproduced by the EMT except for $kD = 2\pi$, where we clearly see how

24

the spectrum predicted by the EMT contains a significantly higher level of energy mainly concentrated at the subharmonic. In Figure 13, we show that optimal subharmonic emission conditions appears for $k_{ext}D = [0.65, 0.75]\pi$ as a consequence of the crystal configuration. This effect is not captured by the EMT.

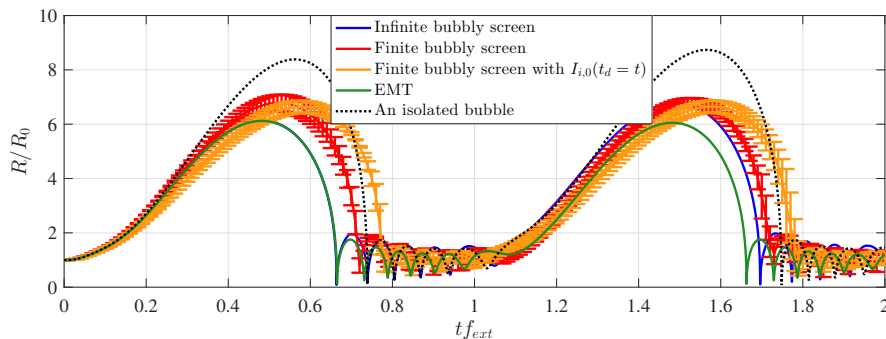### 2. Strongly non-linear regime

FIG. 14. Radius versus time curves predicted by different models for $\omega_{ext}/\omega_0 = 0.1$, $p_a/p_0 = 2$, $D/R_0 = 134$ for an infinite bubbly screen oscillating synchronously and a 11×11 bubbly screen. In the later case, we show the averaged and the standard deviation of the bubble radius using the full model (red line) and the incompressible model wtih $I_i = I_{i,0}$ and $t_d = t$ (yellow line).

When the excitation frequency is decreased $(\omega_{ext}/\omega_0 = 0.1)$ the response of the bubbles become highly non-linear with a clear distinction between the expansion phase and the collapse and rebound region. In order to reduce the simulation time and transient effects, in this section we excite a bubbly screen with a perfect crystal configuration with an incident
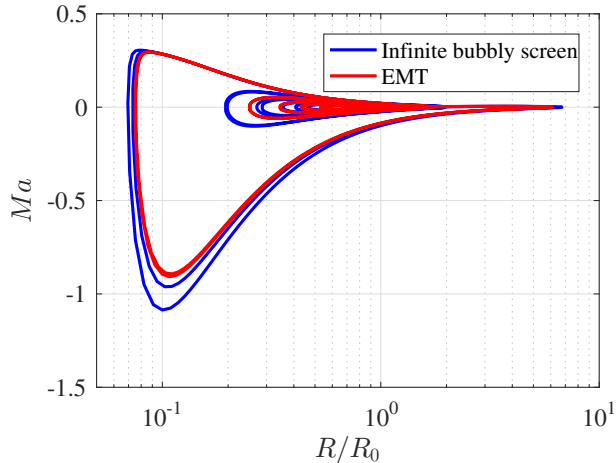
25

FIG. 15.   Comparison of the trajectory of the averaged bubble radius versus $Ma = \dot{R}/c$ for the current model and the EMT.

planar wave represented by

$$p_\infty\left(t\right) = p_0 - p_a \sin(\omega_{ext} t).$$

The predictions of the temporal evolution of the bubble radius predicted by different models are given in Figure 14 for both infinite bubbly screens and finite bubbly screens. The amplitude of the initial expansion in all cases is decreased compared to the isolating oscillating bubble. The results from the EMT fit well the results of the infinite bubbly screen in the first expansion. The difference of the radial dynamics between different models appear in the rebound stage (Figure 15), when the Mach number($\dot{R}/c$) becomes important, so does the first order compressibility correction terms.

For completeness, in Figure 14 we also include the full simulation of a 11×11 bubbly screens. Because in this case bubble motion is no longer assumed to be synchronous, we

26

represent the averaged bubble radius among all bubbles in the screen as well as the standard deviation in one realization. The influence of the screen is reduced in the expansion and is less strong than in the infinite case. Compressible effects play a visible role despite the long wavelength of the incident wave, and the classical incompressible bubble interaction model tends to over-predict the collapse time.

V. CONCLUSION

In this work, the compressibility effect on the bubble-bubble interaction is discussed. The model proposed in Fuster and Colonius (2011) is particularized to explicitly write a system of equations that account for first order correction compressibility effects. These effects are shown to be important compared with the classical incompressible interaction mechanism in Rayleigh–Plesset models.

In the linear regime, time delay effects are always critical to capture the overall system response of large bubble screens. We show that the current model recovers the effective medium theory results up to second order for infinite crystal structures at large wavelengths $(kD \ll 1)$. In addition, the model is able to capture resonant conditions in diluted systems due to crystal configurations that are not captured by averaged models. Randomization on the bubble position and boundary effects on bubbly screens of finite are shown to be responsible to the appearance of characteristic periodic structures in the screen. These effects can modify the effective damping measured under some conditions.

In the non-linear oscillating regime, we numerically solve the proposed model as a neutral delay-differential set of equations (NDDE). The fully incompressible model seems to be only suitable to predict the expansion phase, while during the strong collapse compressibility effects play a major role and need to be included. Boundary size effects are shown to limit the applicability of the effective medium theory valid only for infinite systems.

ACKNOWLEDGMENTS

APPENDIX A:

The system of equations 4 can be written in matrix form $\mathbf{A}\vec{r} = \vec{B}p'$ after imposing that the incident wave is $p_\infty = p_0(1 + p'e^{\imath\omega t})$ with $p' \ll 1$. The final system of equations becomes

$$\mathbf{A} = \mathbf{A}^{(0)} + \imath k R_0 \mathbf{A}^{(1)} = \vec{B}p'$$

where

$$B_i = -\frac{p_0}{\rho R_0^2 \omega_0^2},$$

$$A_{ij}^{(0)} = \begin{cases} 1 - \left(\frac{\omega}{\omega_0}\right)^2 & \text{if } i = j, \\ -\left(\frac{\omega}{\omega_0}\right)^2 S_{ij} & \text{otherwise,} \end{cases}$$

28

$$
A_{ij}^{(1)} = \begin{cases} \left(\frac{\omega}{\omega_0}\right)^2 (1 + \Re_i) - \Re_i & \text{if } i = j, \\[2ex] \left(\left(\frac{\omega}{\omega_0}\right)^2 (1 + \Re_i) + 1\right) S_{ij} & \text{otherwise,} \end{cases}
$$

with $S_{ij} = \frac{R_0}{D} \frac{e^{-\imath k D \tilde{d}_{ij}}}{\tilde{d}_{ij}}$ and $\Re_i = \sum_{j \neq i}^{N} S_{ij}$.

In a general case where bubbles do not necessarily oscillate synchronously, it is possible to rewrite this system by separating variables S_{ij} and $\Re_i$ into a uniform contribution and a spatially fluctuating part attributed to the perturbation of bubbles position

$$
S_{ij} = S_{ij}^{(c)} + S_{ij}'
$$

,

$$
\Re_i = \Re_i^{(c)} + \Re_i' = \sum_{j \neq i}^{N} S_{ij}^{(c)} + \sum_{j \neq i}^{N} S_{ij}',
$$

where the superscript $^{(c)}$ stands for variables corresponding to the crystal configuration, and and the distances between bubbles is written as $\tilde{d}_{ij} = \tilde{d}_{ij}^{(c)} + \tilde{d}_{ij}'$. In this case matrix $\mathbf{A}$ can be further decomposed as $\mathbf{A} \approx \mathbf{A}^{(C)} + \mathbf{A}'$ where $\mathbf{A}^{(C)}$ represents the value of $\mathbf{A}$ obtained with the values of a crystal structure and $\mathbf{A}'$ is the non-uniform part

$$
A_{ij}'^{(0)} = \begin{cases} 0 & \text{if } i = j, \\[2ex] -\left(\frac{\omega}{\omega_0}\right)^2 S_{ij}' & \text{otherwise,} \end{cases}
$$

$$
A_{ij}'^{(1)} = \begin{cases} \left(\left(\frac{\omega}{\omega_0}\right)^2 - 1\right) \Re_i' & \text{if } i = j, \\[2ex] \left(\left(\frac{\omega}{\omega_0}\right)^2 + 1\right) S_{ij}' + \left(\frac{\omega}{\omega_0}\right)^2 (\Re_i' S_{ij}' + \Re_i^{(c)} S_{ij}' + \Re_i' S_{ij}^{(c)}) & \text{otherwise.} \end{cases}
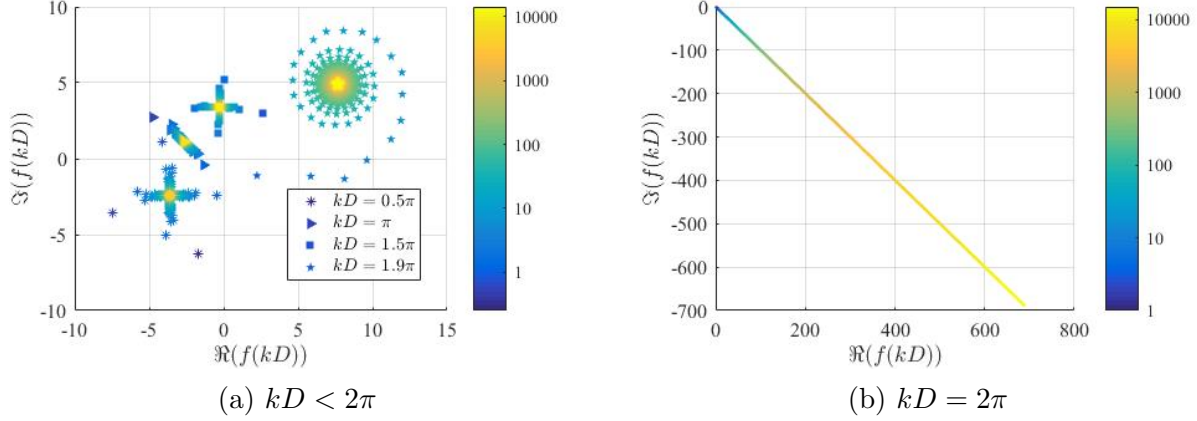$$

FIG. 16. Influence of the truncation N_l on the evaluation of the series in Eq. 13 for a crystal infinite screen and different values of kD. The colorbar is $N_l\frac{D}{\lambda}$.

When the position perturbation is small, taking advantage of Taylor expansion, we have:

$$S'_{ij} \approx -\imath kD\tilde{d}'_{ij}\frac{R_0}{D}\frac{e^{-\imath kD\tilde{d}^{(c)}_{ij}}}{\tilde{d}^{(c)}_{ij}}.$$

351 In such a situation, the expectation of $A'^{(0)}_{ij}$ is zero as long as the expectation of $\tilde{d}'_{ij}$ is zero.

352 However the expectation of the $\mathcal{K}'_i S'_{ij}$ term appearing in $A'^{(1)}_{ij}$, which acts like a variance

353 term, is different from zero even for the small perturbations. Obviously when the amplitude

354 of perturbation $\tilde{d}'_{ij}$ is large, the expectation of both $A'^{(0)}_{ij}$ and $A'^{(1)}_{ij}$ are a-priori different from

355 zero.

356 **APPENDIX B:**

357 The convergence of the infinite series

$$f(kD) = \sum_{l=1}^{\infty}\frac{4}{l}e^{-\imath kDl}\left(1 + \sum_{q=1}^{l}\frac{2}{\sqrt{1+(q/l)^2}}e^{\imath kDl(1-\sqrt{1+(q/l)^2})}\right)$$

30

is discussed as follows. For sufficiently large value of l, because quantity $p = \sqrt{1 + (q/l)^2}$ is

bounded between 1 and $\sqrt{2}$, we can approximate the series as

$$\sum_{q=1}^{l} \frac{2}{\sqrt{1 + (q/l)^2}} e^{\imath k Dl(1 - \sqrt{1 + (q/l)^2})} \approx \int_{1}^{\sqrt{2}} \frac{2}{p} e^{\imath k Dl(1-p)} dp = 2 e^{\imath k Dl} \left(E_{1/2}(\imath k Dl) - 2^{1/4} E_{1/2}(\sqrt{2}\imath k Dl) \right),$$

where $E(x)$ is the exponential integral function. Taking the limit for $l \to \infty$, we readily find

that

$$\lim_{l \to \infty} \left(E_{1/2}(\imath k Dl) - 2^{1/4} E_{1/2}(\sqrt{2}\imath k Dl) \right) = 0$$

implying that this term always converges. The convergence of the series is then discussed

in terms of the convergence of

$$\sum_{l=1}^{\infty} \frac{4}{l} e^{-\imath k Dl} = \sum_{l}^{\infty} \frac{z^l}{l} = \ln \left(\frac{1}{1-z} \right)$$

where $z = e^{-\imath k D}$. For $kD = 2\pi n$ the series diverges and it converges otherwise. The influ-

ence of the number of layers considered on the series is reported in Figure 16 for different

values of kD. In general, a very large value of the number of layers is required to accurately

represent the infinity limit.

Andersen, K. S., and Jensen, J. A. (**2009**). "Ambient pressure sensitivity of microbubbles

investigated through a parameter study," The Journal of the Acoustical Society of America

126(6), 3350–3358.

Bellen, A., and Zennaro, M. (**2013**). *Numerical methods for delay differential equations*

(Oxford university press).

Bremond, N., Arora, M., Ohl, C.-D., and Lohse, D. (**2006**). "Controlled multibubble surface cavitation," Physical review letters **96**(22), 224501.

Caflisch, R. E., Miksis, M. J., Papanicolaou, G. C., and Ting, L. (**1985**). "Effective equations for wave propagation in bubbly liquids," Journal of Fluid Mechanics **153**, 259–273.

Commander, K. W., and Prosperetti, A. (**1989**). "Linear pressure waves in bubbly liquids: Comparison between theory and experiments," The Journal of the Acoustical Society of America **85**(2), 732–746.

Coussios, C. C., and Roy, R. A. (**2008**). "Applications of acoustics and cavitation to noninvasive therapy and drug delivery," Annu. Rev. Fluid Mech. **40**, 395–420.

Dahl, P. H., and Kapodistrias, G. (**2003**). "Scattering from a single bubble near a roughened air–water interface: Laboratory measurements and modeling," The Journal of the Acoustical Society of America **113**(1), 94–101.

Devaud, M., Hocquet, T., and Leroy, V. (**2010**). "Sound propagation in a monodisperse bubble cloud: From the crystal to the glass," The European Physical Journal E **32**(1), 13–23.

Doinikov, A. A., Manasseh, R., and Ooi, A. (**2005**). "Time delays in coupled multibubble systems (l)," The Journal of the Acoustical Society of America **117**(1), 47–50.

Faez, T., Emmer, M., Kooiman, K., Versluis, M., van der Steen, A. F., and de Jong, N. (**2012**). "20 years of ultrasound contrast agent modeling," IEEE transactions on ultrasonics, ferroelectrics, and frequency control **60**(1), 7–20.

Fan, Y., Li, H., and Fuster, D. (**2020**a). "Optimal subharmonic emission of stable bubble oscillations in a tube," Physical Review E **102**(1), 013105.

Fan, Y., Li, H., Zhu, J., and Du, W. (**2020**b). "A simple model of bubble cluster dynamics in an acoustic field," Ultrasonics sonochemistry **64**, 104790.

Foldy, L. L. (**1945**). "The multiple scattering of waves. i. general theory of isotropic scattering by randomly distributed scatterers," Physical review **67**(3-4), 107.

Fuster, D. (**2019**). "A review of models for bubble clusters in cavitating flows," Flow, Turbulence and Combustion **102**(3), 497–536.

Fuster, D., and Colonius, T. (**2011**). "Modelling bubble clusters in compressible liquids," Journal of Fluid Mechanics **688**, 352–389.

Gilmore, F. R. (**1952**). "The growth or collapse of a spherical bubble in a viscous compressible liquid," .

Halldorsdottir, V. G., Dave, J. K., Leodore, L. M., Eisenbrey, J. R., Park, S., Hall, A. L., Thomenius, K., and Forsberg, F. (**2011**). "Subharmonic contrast microbubble signals for noninvasive pressure estimation under static and dynamic flow conditions," Ultrasonic imaging **33**(3), 153–164.

Ida, M., Naoe, T., and Futakawa, M. (**2007**). "Suppression of cavitation inception by gas bubble injection: A numerical study focusing on bubble-bubble interaction," Physical Review E **76**(4), 046309.

Ilinskii, Y. A., Hamilton, M. F., and Zabolotskaya, E. A. (**2007**). "Bubble interaction dynamics in lagrangian and hamiltonian mechanics," The Journal of the Acoustical Society of America **121**(2), 786–795.

Katiyar, A., and Sarkar, K. (**2011**). "Excitation threshold for subharmonic generation from contrast microbubbles," The Journal of the Acoustical Society of America **130**(5), 3137–

3147.

Keller, J. B., and Miksis, M. (**1980**). "Bubble oscillations of large amplitude," The Journal of the Acoustical Society of America **68**(2), 628–633.

Lauterborn, W., and Cramer, E. (**1981**). "Subharmonic route to chaos observed in acoustics," Physical Review Letters **47**(20), 1445.

Lauterborn, W., and Koch, A. (**1987**). "Holographic observation of period-doubled and chaotic bubble oscillations in acoustic cavitation," Physical Review A **35**(4), 1974.

Lauterborn, W., and Kurz, T. (**2010**). "Physics of bubble oscillations," Reports on progress in physics **73**(10), 106501.

Leroy, V., Strybulevych, A., Lanoy, M., Lemoult, F., Tourin, A., and Page, J. H. (**2015**). "Superabsorption of acoustic waves with bubble metascreens," Physical Review B **91**(2), 020301.

Leroy, V., Strybulevych, A., Scanlon, M., and Page, J. (**2009**). "Transmission of ultrasound through a single layer of bubbles," The European Physical Journal E **29**(1), 123–130.

Lohse, D. (**2018**). "Bubble puzzles: From fundamentals to applications," Physical review fluids **3**(11), 110504.

Lombard, O., Barrière, C., and Leroy, V. (**2015**). "Nonlinear multiple scattering of acoustic waves by a layer of bubbles," EPL (Europhysics Letters) **112**(2), 24002.

Maeda, K., and Colonius, T. (**2019**). "Bubble cloud dynamics in an ultrasound field," Journal of fluid mechanics **862**, 1105.

Manasseh, R., Nikolovska, A., Ooi, A., and Yoshida, S. (**2004**). "Anisotropy in the sound field generated by a bubble chain," Journal of Sound and Vibration **278**(4-5), 807–823.

34

Mettin, R., Akhatov, I., Parlitz, U., Ohl, C., and Lauterborn, W. (**1997**). "Bjerknes forces between small cavitation bubbles in a strong acoustic field," Physical review E **56**(3), 2924.

Miksis, M. J., and Ting, L. (**1989**). "Effects of bubbly layers on wave propagation," The Journal of the Acoustical Society of America **86**(6), 2349–2358.

Nio, A. Q., Faraci, A., Christensen-Jeffries, K., Raymond, J. L., Monaghan, M. J., Fuster, D., Forsberg, F., Eckersley, R. J., and Lamata, P. (**2019**). "Optimal control of sonovue microbubbles to estimate hydrostatic pressure," IEEE transactions on ultrasonics, ferroelectrics, and frequency control **67**(3), 557–567.

Okita, K., Sugiyama, K., Takagi, S., and Matsumto, Y. (**2013**). "Microbubble behavior in an ultrasound field for high intensity focused ultrasound therapy enhancement," The Journal of the Acoustical Society of America **134**(2), 1576–1585.

Ooi, A., Nikolovska, A., and Manasseh, R. (**2008**). "Analysis of time delay effects on a linear bubble chain system," The Journal of the Acoustical Society of America **124**(2), 815–826.

Pham, K., Mercier, J.-F., Fuster, D., Marigo, J.-J., and Maurel, A. (**2021**). "Scattering of acoustic waves by a nonlinear resonant bubbly screen," Journal of Fluid Mechanics **906**.

Prosperetti, A., Lezzi, A. *et al.* (**1986**). "Bubble dynamics in a compressible liquid. part 1. first-order theory.," J. FLUID MECH., 1986, **168**, 457–478.

Shampine, L. (**2005**). "Solving odes and ddes with residual control," Applied Numerical Mathematics **52**(1), 113–127.

Shampine, L. F. (**2008**). "Dissipative approximations to neutral ddes," Applied Mathematics and Computation **203**(2), 641–648.

[458] Sujarittam, K., and Choi, J. J. (**2020**). "Angular dependence of the acoustic signal of a

[459] microbubble cloud," The Journal of the Acoustical Society of America **148**(5), 2958–2972.

[460] van't Wout, E., and Feuillade, C. (**2021**). "Proximity resonances of water-entrained air

[461] bubbles near acoustically reflecting boundaries," The Journal of the Acoustical Society of

[462] America **149**(4), 2477–2491.

[463] Yasui, K., Iida, Y., Tuziuti, T., Kozuka, T., and Towata, A. (**2008**). "Strongly interacting

[464] bubbles under an ultrasonic horn," Physical Review E **77**(1), 016609.

[465] Ye, Z., and Feuillade, C. (**1997**). "Sound scattering by an air bubble near a plane sea

[466] surface," The Journal of the Acoustical Society of America **102**(2), 798–805.